Partitioning of energy in highly polydisperse granular gases

H. Uecker,[1,2] W. T. Kranz,[1,3] T. Aspelmeier,[1,3] and A. Zippelius[1,3]

[1] *Institute of Theoretical Physics, University of Göttingen, Friedrich-Hund-Platz 1, 37077 Göttingen, Germany*

[2] *Mathematics and Biosciences Group, Faculty of Mathematics, University of Vienna, Nordbergstrasse 15, A-1090 Vienna, Austria*

[3] *Max Planck Institute for Dynamics and Self Organization, Bunsenstr. 10, 37073 Göttingen, Germany*

(Dated: October 12, 2009)

A highly polydisperse granular gas is modeled by a continuous distribution of particle sizes, a, giving rise to a corresponding continuous temperature profile, $T(a)$, which we compute approximately, generalizing previous results for binary or multicomponent mixtures. If the system is driven, it evolves towards a stationary temperature profile, which is discussed for several driving mechanisms in dependence on the variance of the size distribution. For a uniform distribution of sizes, the stationary temperature profile is nonuniform with either hot small particles (constant force driving) or hot large particles (constant velocity or constant energy driving). Polydispersity always gives rise to non-Gaussian velocity distributions. Depending on the driving mechanism the tails can be either overpopulated or underpopulated as compared to the molecular gas. The deviations are mainly due to small particles. In the case of free cooling the decay rate depends continuously on particle size, while all partial temperatures decay according to Haff's law. The analytical results are supported by event driven simulations for a large, but discrete number of species.

PACS numbers: 45.70.-n, 47.57.Gc, 47.45.Ab

I. INTRODUCTION

Granular media are an important and popular subject of current research which is owed partly to the striking phenomena they reveal and partly to their ubiquity in nature and in industry which makes a good understanding of their properties indispensable [1, 2, 3]. Of special interest are mixtures of different species, as real granular materials such as sand, gravel or seeds are rarely composed of identical particles.

Starting with Jenkins and Mancini [4, 5] *binary* mixtures and in particular their kinetic temperature and transport properties received considerable interest [6, 7, 8, 9, 10, 11, 12, 13, 14]. These studies confirmed that equipartition of energy is indeed violated in granular binary mixtures, an observation that was first made in experiments by Losert *et. al.* [15]. *Polydisperse* granular mixtures, i.e., mixtures composed of more than two types of particles were studied much less [16, 17, 18, 19, 20, 21] although they are closer to realistic systems. In particular, Dahl *et. al.* [17] and Zhi-Yuan *et. al.* [21] simulated mixtures of particles with a distribution of sizes, and Lambiotte *et. al.* [19] discuss mixtures of Maxwell molecules with varying coefficients of restitution.

Out of the many fascinating phenomena inherent to granular mixtures and the observables that are necessary to understand them, we will focus on the partitioning of energy and how it evolves in time, both in the homogeneous cooling state (HCS) and in homogeneously driven systems. Even though, in this paper we will first develop the machinery to deal with an arbitrary number, X, of species, we will eventually go one step further and consider highly polydisperse systems, where no two particles are alike but instead possess properties that are drawn from continuous probability distributions.

In the following three sections we give a short introduction to the model and methods we use. In section V we investigate the temperature in a highly polydisperse system, characterized by a continuous distribution of particle sizes. We finish with a brief conclusion and delegate all technical material to the appendices.

II. MODEL AND OBSERVABLES

In order to model a polydisperse granular gas, we consider mixtures of X different species of smooth inelastic hard spheres. Each species $\alpha = 1, 2, \ldots, X$ consists of $N_\alpha \to \infty$ identical particles, such that the concentrations $x_\alpha := N_\alpha/N$ ($N = \sum_\alpha N_\alpha$) as well as the density $n = N/V$ remain finite as $N_\alpha \to \infty$. Collisions between particles are assumed to be instantaneous and the particles move freely between collisions. Because of the vanishing collision time collisions of more than two particles can be neglected, i.e. the dynamics is determined by two particle collisions. The inelasticity is described by a velocity independent coefficient of normal restitution, $\epsilon_{\alpha\beta} \in [0, 1]$, which may depend on the pair of species $\alpha, \beta = 1, 2, \ldots, X$ that the colliding particles belong to:

$$\hat{\boldsymbol{n}} \cdot \boldsymbol{v}'_{12} = -\epsilon_{\alpha\beta} \hat{\boldsymbol{n}} \cdot \boldsymbol{v}_{12}, \tag{1}$$

where $\boldsymbol{v}_{12} = \boldsymbol{v}_1 - \boldsymbol{v}_2$ is the relative velocity of the colliding particles at contact before the collision and $\boldsymbol{v}'_{12}$ the corresponding quantity after the collision. The unit vector $\hat{\boldsymbol{n}}$ points from the center of particle 1 to the center of particle 2. Apart from the mutual coefficient of restitution $\epsilon_{\alpha\beta}$, the species may also differ in mass m_α and in size (radius) a_α.

The collision law [eq. (1)] together with conservation of momentum determines the postcollisional velocities $\boldsymbol{v}_1'$ and $\boldsymbol{v}_2'$ uniquely in terms of the precollisional ones ($\boldsymbol{v}_1$, $\boldsymbol{v}_2$):

$$\begin{aligned} \boldsymbol{v}_1' &= \boldsymbol{v}_1 - \frac{m_2}{m_1+m_2}(1+\epsilon_{12})(\hat{\boldsymbol{n}}\cdot\boldsymbol{v}_{12})\hat{\boldsymbol{n}}, \\ \boldsymbol{v}_2' &= \boldsymbol{v}_2 + \frac{m_1}{m_1+m_2}(1+\epsilon_{12})(\hat{\boldsymbol{n}}\cdot\boldsymbol{v}_{12})\hat{\boldsymbol{n}} \end{aligned} \tag{2}$$

As we consider smooth spheres the tangential component of the relative velocity ($\boldsymbol{v}_{12}\times\hat{\boldsymbol{n}}$) remains unaffected.

Due to the inelasticity, the particles suffer an energy loss during collision, i.e. the gas will cool down. To compensate for this energy loss, one can provide the system with external energy. We will restrict ourselves to volume driving [22]: With a given frequency f_{dr} random kicks

$$\boldsymbol{p}_i \to \boldsymbol{p}_i + p_{\mathrm{dr}}\boldsymbol{\xi}_i(t) \tag{3}$$

are applied to all particles individually ($\boldsymbol{p}_i \equiv m_i\boldsymbol{v}_i$). The strength of the kicks is controlled by p_{dr} while the components of $\boldsymbol{\xi}_i$ are drawn form a white noise source: $\overline{\xi_i^a}=0$ and $\overline{\xi_i^a(t)\xi_j^b(t')}=\delta_{ij}\delta^{ab}\delta(t-t')$. The time between two driving events is taken to be small compared to the time scale on which the gas would cool down without energy supply.

When considering X-component mixtures, the driving strength p_{dr} may in general be a function of the particle species $p_{\mathrm{dr}}\equiv p_{\mathrm{dr}}^{\alpha}$. There are several experimental methods (both in $D=2$ and $D=3$) that one can hope to describe approximately by volume driving: Shaking on a rough plate [23], electrostatic [24, 25] or magnetic [25, 26] excitation, fluidisation by air [27, 28] or water [29]. As it is not obvious how to best describe the driving of all these experiments theoretically, we propose the following three simple mechanisms:

i. force controlled driving, assuming that all particles experience the same force ($p_{\mathrm{dr}}^{\alpha}\equiv p_{\mathrm{dr}}$),

ii. velocity controlled driving, assuming that all particles get velocity kicks of the same magnitude ($p_{\mathrm{dr}}^{\alpha}\propto m_{\alpha}$) and

iii. energy controlled driving, supplying every species on average with the same energy ($p_{\mathrm{dr}}^{\alpha}\propto m_{\alpha}^{1/2}$).

The first two mechanisms combined with an additional viscous drag force $\propto\eta\boldsymbol{v}$ are also discussed in the context of binary mixtures by Pagnani *et. al.* [10]. Our hope is that the results discussed below may help to clarify the experimental conditions.

The basic quantity of interest is the one-particle velocity distribution, $f_\alpha(\boldsymbol{v})\mathrm{d}^Dv$, of species α which is related to the one-particle distribution $f_\alpha(\boldsymbol{r},\boldsymbol{v})\mathrm{d}^Dr\mathrm{d}^Dv$ by $f_\alpha(\boldsymbol{v})=\int f_\alpha(\boldsymbol{r},\boldsymbol{v})\mathrm{d}^Dr$. As an example, consider species that differ in mass, so that the one-particle velocity distribution is explicitly given by

$$f_\alpha(\boldsymbol{v})\mathrm{d}^Dv = \sum_i^N \delta_{m_i,m_\alpha}\langle\delta(\boldsymbol{v}-\boldsymbol{v}_i)\rangle\,\mathrm{d}^Dv,$$

where the angular brackets $\langle\cdot\rangle$ denote the average over the N-particle distribution function. It is normalized such that

$$\int \mathrm{d}^Dv\, f_\alpha(\boldsymbol{v}) = N_\alpha \quad\text{and}\quad \sum_\alpha\int \mathrm{d}^Dv\, f_\alpha(\boldsymbol{v}) = N.$$

The partial granular temperature for species α in D space dimensions is defined by

$$\frac{D}{2}T_\alpha := \frac{1}{N_\alpha}\sum_i \frac{m_\alpha}{2}\left\langle v_i^2\right\rangle\delta_{m_i,m_\alpha} = \frac{\int \mathrm{d}^Dv\, f_\alpha(\boldsymbol{v})\frac{m_\alpha v^2}{2}}{\int \mathrm{d}^Dv\, f_\alpha(\boldsymbol{v})}. \tag{4}$$

The mean temperature, $\overline{T}=\sum_\alpha x_\alpha T_\alpha$, is then just given by the mean kinetic energy

$$\frac{D}{2}\overline{T} = \frac{1}{N}\sum_\alpha\int \mathrm{d}^Dv\, f_\alpha(\boldsymbol{v})\frac{m_\alpha v^2}{2} = \frac{1}{N}\sum_i\frac{m_i}{2}\langle v_i^2\rangle.$$

The above definitions are easily generalized to other species characteristics, e.g. different size or different coefficients of restitution: The indicator function, δ_{m_i,m_α}, just has to be replaced by the corresponding one.

Our main emphasis in this paper are particles whose properties depend on a continuous variable $\alpha\in\mathbb{R}$ that follows a prescribed probability distribution $d\mu(\alpha)$, i.e.

$$\sum_\alpha \frac{N_\alpha}{N} \to \int \mathrm{d}\alpha\, x(\alpha) = \int \mathrm{d}\mu(\alpha).$$

The temperature becomes a continuous function $T_\alpha\to T(\alpha)$ whose mean and variance is given by

$$\begin{aligned} \overline{T} &= \int T(\alpha)\mathrm{d}\mu(\alpha)\,, \quad \Delta T = \overline{T^2}-\overline{T}^2 \\ &\text{with}\quad \overline{T^2} = \int T^2(\alpha)\mathrm{d}\mu(\alpha). \end{aligned} \tag{5}$$

In our example of a distribution of masses, $\alpha=m$ the one-particle velocity distribution, $f(m,\boldsymbol{v})\mathrm{d}^3v\,\mathrm{d}m$, is defined by

$$f(m,\boldsymbol{v}) = \sum_i^N \delta(m_i-m)\langle\delta(\boldsymbol{v}-\boldsymbol{v}_i)\rangle.$$

III. ANALYTICAL THEORY

The time evolution of the temperatures is computed with the help of the pseudo Liouville operator formalism. For details see e.g. refs. 30 and 31. In this framework the time evolution of an observable A is given by the equation

$$\frac{\mathrm{d}}{\mathrm{d}t}\langle A\rangle = \langle i\mathcal{L}A\rangle,$$

where $i\mathcal{L}$ denotes the pseudo Liouville operator.

The pseudo Liouville operator for the driven hard sphere gas consists of three terms. The term $i\mathcal{L}_0$ describes free streaming which does not affect the temperature, the term $i\mathcal{L}_H$ accounts for driving and $i\mathcal{L}_I$ for interactions between particles. In a gas consisting of X different species one obtains

$$i\mathcal{L} = i\mathcal{L}_0 + i\mathcal{L}_H + \sum_{\alpha=1}^{X}\sum_{\beta=1}^{\alpha} i\mathcal{L}_{\alpha\beta},$$

where $i\mathcal{L}_{\alpha\beta}$ accounts for interactions between particles of species α with particles of species β. For the evolution of the temperature of a particular species, only interactions with participation of that species play a role; collisions between particles of other species do not have a direct influence. Given a discrete number, X, of different species, the temperature of species α, eq. (4), develops in the following way

$$\frac{D}{2}\frac{\mathrm{d}}{\mathrm{d}t}T_\alpha = \langle i\mathcal{L}_H \overline{E}_{kin}(\alpha)\rangle + \sum_{\beta=1}^{X}\langle i\mathcal{L}_{\alpha\beta}\overline{E}_{kin}(\alpha)\rangle. \quad (6a)$$

Given a continuous distribution $d\mu(\alpha)$ of a parameter α, one obtains

$$\frac{D}{2}\frac{\mathrm{d}}{\mathrm{d}t}T(\alpha) = \langle i\mathcal{L}_H \overline{E}_{kin}(\alpha)\rangle + \int\langle i\mathcal{L}_{\alpha\beta}\overline{E}_{kin}(\alpha)\rangle \mathrm{d}\mu(\beta). \quad (6b)$$

At this point we would like to stress that the above equations hold subject to arbitrary initial conditions $T_\alpha(t = 0)$. The *a priori* assumption of a (quasi-)stationary state that is required for some of the hydrodynamic theories is not needed here.

For a hard core potential the interaction terms $i\mathcal{L}_{\alpha\beta}$ separate into a sum of two particle interaction operators $i\mathcal{L}_{\alpha\beta} = \frac{1}{2}\sum_{k,l} i\mathfrak{T}_{\alpha\beta}^{(kl)}$ with one particle belonging to species α, the other one to species β. For the operator $i\mathfrak{T}_{\alpha\beta}^{(kl)}$ one obtains

$$i\mathfrak{T}_{\alpha\beta}^{(kl)} := -(\boldsymbol{v}_{kl}\cdot\hat{\boldsymbol{n}})\Theta(-\boldsymbol{v}_{kl}\cdot\hat{\boldsymbol{n}})\delta(r_{kl} - a_k - a_l)(b_{\alpha\beta}^{(kl)} - 1),$$

where $b_{\alpha\beta}^{(kl)}$ is the operator replacing the particles' velocities before collision by their values afterwards according to equation (2).

When calculating the phase space average, one has to take into account the excluded volume effect which arises due to the fact that particles cannot overlap. Consequently, the phase space element in D dimensions is given by

$$\mathrm{d}\Gamma = \prod_{i<j}\Theta(r_{ij} - a_i - a_j)\prod_{k=1}^{N_1}\mathrm{d}^D r_k \mathrm{d}^D v_k \cdots \prod_{\ell=1}^{N_X}\mathrm{d}^D r_\ell \mathrm{d}^D v_\ell$$

with r_{ij} the distance between particles i an j.

We assume that the particles are uniformly distributed in space, that the species are well mixed and that velocity correlations between different particles can be neglected (molecular chaos assumption). Under these premises the N-particle distribution function $f_N(\{\boldsymbol{r}_i\},\{\boldsymbol{v}_i\},t)$ factorizes into a product of N single particle distribution functions $f(\boldsymbol{r},\boldsymbol{v},t)$. In a monodisperse system, the single particle distribution function can be written in rescaled form

$$f(\boldsymbol{r},\boldsymbol{v},t) \propto \frac{n}{T(t)^{D/2}}\tilde{f}(\boldsymbol{v}/\sqrt{T(t)})$$

both in the homogeneous cooling state as well as in the stationary state of a driven system [32].

Contrary to elastic gases, a Gaussian distribution is only an approximate solution in the inelastic case. Deviations have been studied extensively for driven and undriven monodisperse systems. Investigations have shown that while a Gaussian approximation is quite good in the range of typical velocities, high velocities are overrepresented in granular gases [32, 33, 34, 35, 36]. In ref. 6 qualitatively similar deviations have been found for freely cooling binary mixtures. The corrections have, however, only little influence on the temperature and the cooling rate [32]. Thus, we make a Gaussian ansatz for the velocity distribution of a single species α with temperature T_α. The N-particle distribution for a mixture with X components then follows:

$$f_N(\{\boldsymbol{r}_i\},\{\boldsymbol{v}_i\},t) \propto \prod_{i=1}^{N_1} e^{-\frac{m_1\boldsymbol{v}_i^2}{2T_1(t)}} \cdots \prod_{j=1}^{N_X} e^{-\frac{m_X\boldsymbol{v}_j^2}{2T_X(t)}}. \quad (7)$$

In undriven systems, the HCS is maintained only for a certain time until velocity correlations develop and clusters form because of the system's instability against density fluctuations [37, 38, 39]. In inelastic mixtures cluster formation is additionally accompanied by the onset of segregation [12, 40]. Therefore our results will in this case be limited to the initial development.

Using the distribution function, eq. (7), evaluation of the term $\langle i\mathcal{L}_{\alpha\beta}\overline{E}_{kin}(\alpha)\rangle$ yields (cf. appendix A):

$$\langle i\mathcal{L}_{\alpha\beta}\overline{E}_{kin}(\alpha)\rangle = -2x_\beta\mu_{\alpha\beta}G_{\alpha\beta}\sqrt{\frac{T_\alpha m_\beta + T_\beta m_\alpha}{2m_\beta}}\left[\frac{A_{\alpha\beta}}{m_\alpha}T_\alpha - \frac{B_{\alpha\beta}}{m_\beta}(T_\beta - T_\alpha)\right] \quad (8)$$

with the reduced mass $\mu_{\alpha\beta} := m_\alpha m_\beta/(m_\alpha + m_\beta)$. The other constants are given by

$$A_{\alpha\beta} := \frac{1-\epsilon_{\alpha\beta}^2}{4}, \quad B_{\alpha\beta} := \frac{1}{4}\frac{(1+\epsilon_{\alpha\beta})^2}{1+\frac{m_\alpha}{m_\beta}}$$

and

$$G_{\alpha\beta} := 4(a_\alpha + a_\beta)n\sqrt{\frac{\pi}{m_\alpha}}\chi_{\alpha\beta} \quad \text{for } D = 2,$$
$$G_{\alpha\beta} := 8(a_\alpha + a_\beta)^2 n\sqrt{\frac{\pi}{m_\alpha}}\chi_{\alpha\beta} \quad \text{for } D = 3$$

where $\chi_{\alpha\beta}$ is the value of the pair correlation function $g_{\alpha\beta}(r)$ at contact. In the following, we will use the approximation $\chi_{ra} = 1$ which is well justified for dilute systems.

The terms in equation (8) have a direct physical interpretation: The factor before the square brackets defines an effective collision frequency $\omega_{\alpha\beta}$ of particles coming from possibly different species with different temperatures. The first term inside the brackets accounts for the dissipation in collisions between α and β particles while the second term describes the heat flux between species with different temperatures which tends to equalize the two temperatures. This term is the only one present in mixtures of elastically colliding particles, where it ensures equipartition. The difference to the elastic cases consists in the dissipative terms. As the cooling rates $\propto G_{\alpha\beta}A_{\alpha\beta}$ are in general different for each species and are completely independent from the rate of energy exchange $\propto G_{\alpha\beta}B_{\alpha\beta}$ they constantly drive the system away from equipartition. The new quasi-stationary state is then no longer characterized by equipartition but by *equal cooling rates* $\dot{T}_\alpha/T_\alpha = \dot{T}_\beta/T_\beta$ [6]. A related interpretation has been given before by Alam and Luding [13]. Moreover it is also apparent that driving the system will in general not be sufficient to restore equipartition as was first shown by Barrat and Trizac [8]. For the special case of an undriven system that already reached its quasi-stationary state, equation (6a) is equivalent to equation (2.4) of ref. 20a.

The driving power H_α which was formally written as $H_\alpha = \langle i\mathcal{L}_H \overline{E}_{kin}(\alpha)\rangle$ in equations (6a) and (6b) can be more easily calculated directly form the definition [eq. (3)]:

$$H_\alpha = f_{\rm dr}(p^\alpha_{\rm dr})^2/2m_\alpha.$$

In particular we get for (i) force controlled driving $H^{\rm fc}_\alpha \propto 1/m_\alpha$, (ii) velocity controlled driving $H^{\rm vc}_\alpha \propto m_\alpha$, and (iii) constant energy input $H^{\rm ec}_\alpha$ independent of m_α.

IV. SIMULATIONS

In order to test our analytical theory we performed complementary computer simulations based on an event-driven (ED) algorithm [41]. Although our code can easily handle up to 10^6 particles, we usually found 10^4 particles per species sufficient for the measurements reported here. Because of the extremely low densities used in this paper, we hardly ever need to take care of the inelastic collapse occurring in ED-simulations. If necessary we use the method of ref. 42 to avoid inelastic collapse.

For monodisperse systems, the minimal cluster size L_c can be derived from a hydrodynamic stability analysis [38, 43]. To keep our systems from clustering, we chose a system size $L \lesssim L_c/6$. Although L_c will certainly be somewhat different for polydisperse systems, we found no indications for clustering or segregation in our simulations.

As mentioned above, our simulations include volume driven systems. In this context it is necessary that the simulation process takes the conservation of momentum into account. To do so, a driving event always concerns two particles at the same time [53]. One of these particles, say particle 1, is chosen at random. The neighborhood of this particle is examined to find the particle, i, closest to the first one. Particles 1 and i are then kicked at the same time t. While a momentum increment $p_{\rm dr}\boldsymbol{\xi}(t)$ [see eq. (3)] is *added* to particle 1, it is *subtracted* from particle i, i.e.

$$\begin{aligned}\boldsymbol{p}_1 &\to \boldsymbol{p}_1 + p_{\rm dr}\boldsymbol{\xi}\\ \boldsymbol{p}_i &\to \boldsymbol{p}_i - p_{\rm dr}\boldsymbol{\xi}\end{aligned}.$$

In that way momentum is conserved on length scales ℓ of a mean particle separation, i.e., $\ell \propto n^{-1/D}$.

The simulations were performed in two steps. Initially the particles were placed on a grid and random velocities drawn from a Gaussian distribution were assigned to the particles. In the first half of the simulation, all coefficients of restitution were set to unity and the elastic mixture was simulated for about 120 collisions per particle to generate a well mixed state. In the next step the desired inelasticities were switched on and the temperatures were recorded until reliable estimates for the stationary values of the observables could be obtained. For the driven systems we chose the driving frequency $f_{\rm dr}$ to be approximately the same as the collision frequency at the desired stationary temperature T_∞. As a compromise between computational efficiency and the desire to reduce temperature fluctuations due to rare but strong driving events this choice of driving frequency was also found satisfactory by Bizon *et. al.* [44].

V. HIGHLY POLYDISPERSE SYSTEMS

Many real granular systems are highly polydisperse with no single particle being identical in shape and size to another one. To account for a high degree of polydispersity we generalize the considerations for polydisperse mixtures to mixtures containing "infinitely" many species. In principle, a variety of scenarios can be thought of and treated within our analytical approach. Here, we will restrict ourselves to the relatively simple case where the particles' radius is uniformly distributed in a range $[R_1, R_2]$; the particles all have the same mass density ρ and all restitution coefficients are equal $\epsilon_{\alpha\beta} \equiv \epsilon$. We furthermore choose units such that $\rho = 1$.

The following questions are of particular interest. Is there a stationary temperature profile, $T(a)$, if the sys-

tem is driven? If so, how does this function reflect the properties of the distribution of radii? How does the forcing mechanism affect the stationary temperature profile? How does the system cool freely if undriven?

Combining equations (6b) and (8) leads to the following integro-differential equation for the temperature of species with radius a:

$$\frac{D}{2}\frac{\mathrm{d}}{\mathrm{d}t}T(a) = H(a) + \mathsf{F}[T](a) \tag{9}$$

where the nonlinear integral operator F is given (in $D = 3$) by

$$\mathsf{F}[T](a) := \frac{n\sqrt{6}}{R_2 - R_1}\int_{R_1}^{R_2} \mathrm{d}r \chi_{ra}\frac{r^3(a+r)^2}{r^3+a^3}\sqrt{\frac{T(a)}{a^3}+\frac{T(r)}{r^3}}\left\{(\epsilon^2-1)T(a) + (1+\epsilon)^2\frac{a^3}{a^3+r^3}\left[T(r)-T(a)\right]\right\}.$$

When the system is driven constantly in time, we expect a stationary temperature profile $T_\infty(a) = T(a, t\to\infty)$, to develop. If this is correct, it should be given as the asymptotic solution of equation (9) with the left hand side set to zero:

$$\mathsf{F}[T_\infty](a) = -H(a) \tag{10}$$

In general T_∞ depends not only on a but also on the two parameters R_1, R_2 of the distribution of radii. By scaling all radii with R_1, one observes that (up to a scale factor) T_∞ depends only on the ratios $a^* = a/R_1$ and $R = R_2/R_1$, but not on the absolute values. Alternatively, we choose a^* and the relative width of the distribution $\Delta = 2(R_2 - R_1)/(R_2 + R_1)$ as independent variables: $T_\infty = T_\infty(a^*, \Delta)$.

We solved the above nonlinear integral equation (10) numerically by applying Banach's fixed point iteration (for details see appendix B). We always found a solution, confirming that a stationary temperature profile is indeed reached for asymptotically long times.

Independently, we performed event driven simulations and measured all the partial temperatures $T(a, t)$. The amount of simulation time needed for sufficiently good statistics quickly rises with the number of species. To this end, we checked if a *highly polydisperse* system can be approximated by a *polydisperse* mixture with many species such that there is still a considerable number of particles for each species. Considering equation (6a) for increasing numbers of species we found that the temperatures considered in this paper rapidly converge. Figure 1(a) shows how mixtures of respectively three and five species compare to the result for a continuous distribution. From these results we conclude that considering $X = 20$–30 species for the simulations should yield results practically indistinguishable from the highly polydisperse case.

In FIG. 2 we show the stationary temperature $T_\infty(a^*, \Delta)$ as a function of particle radius a^* for the three driving mechanisms proposed in section II. The

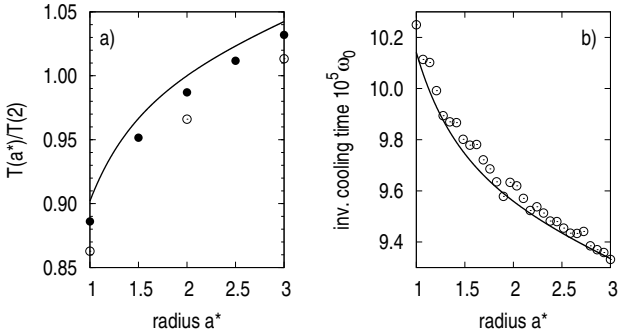

FIG. 1: a) The stationary temperatures [eqs. (6a) & (6b)] in a three component (open disks) and five component (filled disks) mixtures compared to those of a highly polydisperse mixture for energy controlled driving $H^{\mathrm{ec}} = 10^{-3}$ at density $n = 5\times10^{-4}$ and coefficient of restitution $\epsilon = 0.9$. b) Inverse cooling time ω_0 in a two dimensional system for a uniform size distribution of width $R = 3$, coefficient of restitution $\epsilon = 0.9$ and density $n = 2\times10^{-4}$. The symbols denote simulation results for $X = 30$ species each with 10^4 particles, while the solid line is the solution of eq. (12).

rough trends can be understood from the following qualitative arguments. Force controlled driving $H^{\mathrm{fc}}(a^*) \propto 1/m(a^*) \propto a^{*-3}$ is dominant for small particles so that one expects the partial temperatures, $T_\infty(a^*, \Delta)$, to decrease with increasing size a^*. This is indeed born out by the solution of the integral equation (10) and supported by simulations, which are seen to agree well with the theoretical result. Velocity controlled driving $H^{\mathrm{vc}} \propto m(a^*)$ is dominant for large particles so that we expect the partial temperatures to increase with increasing size of the particles, as is indeed observed in FIG. 2. Finally, for the energy controlled mechanism, $H^{\mathrm{ec}}(a^*) \equiv H$, is independent of the particle size, nevertheless $T_\infty(a^*, \Delta)$ depends weakly on a^*. One has to keep in mind that all the species interact and that this will lead to nontrivial conditions of stationarity as in the binary case. These effects are

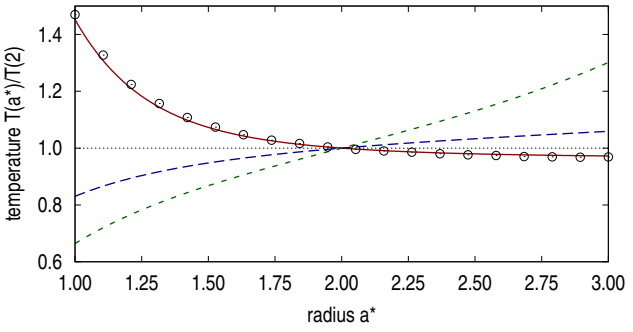

FIG. 2: (Color online) The stationary temperature in a three dimensional driven system for a size distribution with $R_2 = 3R_1$, a coefficient of restitution $\epsilon = 0.9$ at a density $n = 2\times10^{-4}$. Force controlled driving $H^{\rm fc}(a) = 1.875\times10^{-3}/m(a)$ (solid, red), energy controlled driving $H^{\rm ec} = 1.875 \times 10^{-3}$ (long dashed, blue) and velocity controlled driving $H^{\rm vc}(a) = 1.875 \times 10^{-3}m(a)$ (short dashed, green). For the simulation data (symbols) a system of 20 different particle species with 10^4 particles each was used.

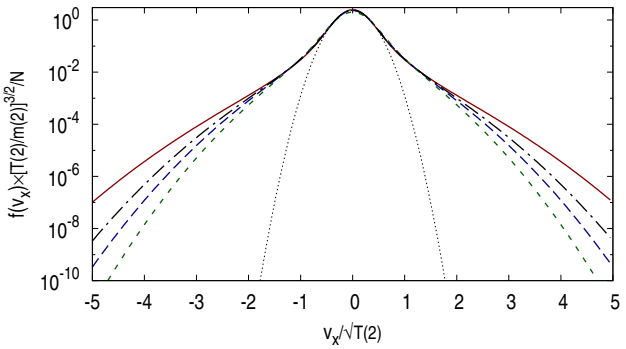

FIG. 3: (Color online) Stationary velocity distribution [eq. (11)] in a three dimensional driven system; parameters and symbols as in FIG. 2; for comparison the velocity distribution of an elastically colliding, molecular gas (dashed-dotted, black) and a gaussian fit to the central part of the distribution (thin dotted line) are also shown.

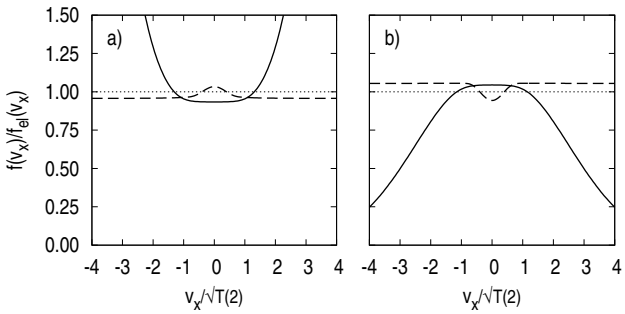

FIG. 4: Stationary velocity distribution relative to the elastic gas and separately for the two halves of smaller (full line) and larger (dashed line) particles; parameters as in FIG. 2; a) force controlled driving, b) energy controlled driving.

responsible for the precise functional form of the temperature profile which goes beyond the simple rough trend for all three driving mechanisms. The same trends for force controlled versus velocity controlled driving have been found by Pagnani *et. al.* [10] in the case of binary mixtures.

Abate and Durian [28] discuss several systems that, although they are comprised of only two to five particles come close to our definition of highly polydisperse systems in that no two particles are alike. Two spheres of different sizes show a marked increase in the temperature ratio with increasing size ratio. This would roughly correspond to our results for velocity controlled driving but the authors of ref. 28 observed a complicated two particle interaction. Moreover, they considered a system with five different spheres of the same size but different densities. Based on the results from binary mixtures one infers that the effects of different masses is much stronger than that of different sizes. If this reasoning is valid the weak dependence of the temperature on the mass would correpond to energy controlled driving in the present paper.

Within our approximation scheme, the partial temperatures (i.e., the temperature profile), $T_\infty(a^*)$, determine the one-particle velocity distribution according to

$$f(a,\boldsymbol{v}) = \frac{N}{R_2 - R_1}\left[\frac{m(a)}{2\pi T_\infty(a)}\right]^{D/2} e^{-m(a)\boldsymbol{v}^2/2T_\infty(a)}.$$

The total velocity distribution, $f(\boldsymbol{v})\mathrm{d}^3v$ is thus given by

$$f(\boldsymbol{v}) = \int_{R_1}^{R_2} \mathrm{d}a f(a,\boldsymbol{v}). \qquad (11)$$

This function is in general not Gaussian, not even for an elastic molecular gas with many different species. In FIG. 3 we show the total velocity distribution as given by equation (11). The elastic system (dashed-dotted) is compared to the inelastic gas with different driving mechanisms. In comparison to the molecular gas the tails of the velocity distribution can either be overpopulated, as observed for force controlled driving (solid line), or underpopulated for energy (long dashed) or velocity controlled (short dashed) driving.

To clearly see the difference to the elastic case, we plot in FIG. 4 the velocity distribution relative to the elastic gas. We furthermore separate the particles into two halves, one with the smaller and one with the larger particles. The strongest deviations are clearly in the tails and solely due to the small particles. The velocity distribution of the large particles has almost the same form as in the elastic gas, except for very small velocities. Force and energy controlled driving are almost mirror images of each other — even for the detailed structures at small velocities.

How does the temperature profile, $T_\infty(a^*, \Delta)$, reflect the prescribed distribution of radii? The latter is characterized by a single parameter, the relative width Δ, which can take values $0 \le \Delta \le 2$. In FIG. 5 we show

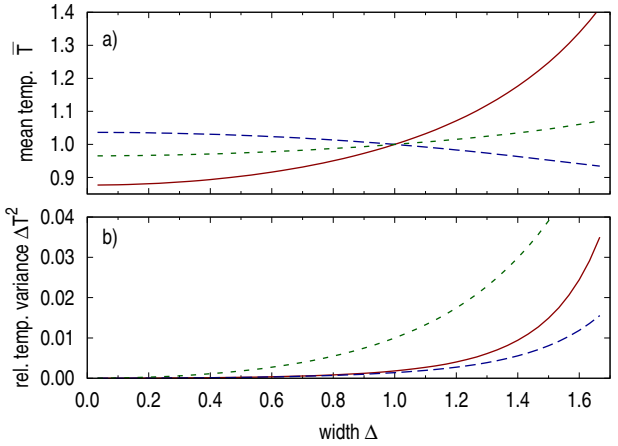

FIG. 5: (Color online) a) The mean temperature $\overline{T}$ [eq. (5)] and b) the relative temperature variance $\Delta T^2 = \overline{T^2}/\overline{T}^2 - 1$ as a function of the relative width of the size distribution Δ for the three driving mechanisms $H^{\rm fc}(a) = 10^{-2}/m(a)$ (solid, red), $H^{\rm ec}(a) = 10^{-2}$ (long dashed, blue) and $H^{\rm vc}(a) = 10^{-2}m(a)$ (short dashed, green), coefficient of restitution $\epsilon = 0.9$ and density $n = 5 \times 10^{-4}$. The mean temperatures in (a) are rescaled such that they agree for a relative width of $\Delta = 1$.

the mean temperature $\overline{T}$ and the temperature variance $\Delta T^2 := \overline{T^2} - \overline{T}^2$ (see eq. (5)) as a function of Δ. In FIG. 5(a) we show the mean temperature $\overline{T}(\Delta)/\overline{T}(1)$, scaled such that they coincide at $\Delta = 1$. Surprisingly the dependence is nonmomotonic for different driving mechanisms: whereas $\overline{T}(\Delta)$ increases with Δ for force and velocity controlled driving, $\overline{T}(\Delta)$ decreases with Δ for energy controlled driving. The strongest variation is observed for force controlled driving. The corresponding variance of the temperature profile [FIG. 5(b)] increases trivially with Δ. The variance for velocity controlled driving is almost an order of magnitude larger than for the other two driving mechanisms.

We next consider the freely cooling case ($H(a) \equiv 0$) [19, 20]. We expect Haff's law [45] to hold also for $T(r,t)$ and hence make the ansatz

$$T(a,t) \propto \omega_0(a)^{-2} t^{-2}$$

for large times. This leads to an integral equation for the inverse cooling time ω_0

$$-D\omega_0^{-2}(a) = \mathsf{F}[\omega_0^{-2}](a) \qquad (12)$$

Similarly to T_∞, the decay rate ω_0 depends only on $a^* = a/R_1$ and $R = R_2/R_1$, or alternatively Δ, but not on the absolute values: $\omega_0 = \omega_0(a^*, \Delta)$. The above integral equation is solved numerically by subsequently applying Banach's fixed point iteration and Newton's method (for details see appendix B). To extract $\omega_0(a^*, \Delta)$ from the simulations, we performed simulations with $X = 30$ species, measured all partial temperatures and fitted them to Haff's law. The resulting decay rates are plotted in FIG. 1(b). The rate is seen to be a monotonically decreasing function of a^*, however the dependence is weak. Since the coefficient of restitution is the same for all particles, this is a pure size effect, implying that smaller particles relax faster than larger ones. The simulation data are seen to agree well with the theoretical results, but show a considerable scatter. This is most likely due to the difficulty in fitting the data to Haff's law, given the uncertainty in time scale, when the asymptotic decay applies.

VI. CONCLUSION

We examined the partitioning of energy in highly polydisperse mixtures of smooth hard spheres. The properties of the particles, such as mass, radius or coefficient of restitution, are chosen from a continuous distribution giving rise to a corresponding continuous temperature profile. The latter has been computed approximately, generalizing previous approaches of mixtures with several species. The analytical theory leads to a nonlinear integro-differential equation for the time dependent temperature profile, which has been solved numerically.

Our results are supported by event driven simulations for mixtures with $X = 20 - 30$ species. The good agreement between ED simulations and the analytical theory indicates that the assumptions of homogeneity and molecular chaos that are fundamental to the theory are indeed observed in the simulated system. The direct simulation monte carlo (DSMC) method [46], otherwise well suited for dilute (granular) gases (see e.g. [47, 48, 49, 50]), would not have been able to show this as it ensures both homogeneity and molecular chaos by construction.

As a specific example we have studied a *uniform* size distribution in detail. We showed that a highly polydisperse mixture still obeys Haff's law during free cooling. The distribution of sizes gives rise to a nonuniform distribution of cooling rates, such that the smaller particles are cooling faster.

A driven system relaxes to a stationary temperature profile which is in general *nonuniform*. Depending on the driving mechanism, its weight can be predominantly at small or large particles. If the particles are driven by a constant force, then the smaller particles are hotter. If the driving process supplies either a constant energy or velocity, then the larger particles have a higher temperature. The temperature profile reflects the distribution of radii, characterized by the relative width Δ. The variance of the temperature increases with Δ, as one would expect, whereas the mean temperature can either increase (constant force driving) or decrease with Δ (constant energy supply).

This strong dependence on the driving mechanism is also observed in the velocity distributions. For a polydisperse system, these are in general weighted sums of all partial distributions and hence in general not Gaus-

sian, even if the partial distributions are Gaussian like in an elastic gas. The velocity distribution in an inelastic, driven gas can have either *overpopulated* or *underpopulated* tails, as compared to the molecular gas. Furthermore, the effects are dominated by the small particles.

Acknowledgments

We thank M. Sperl for carefully reading the manuscript and M. Schröter for valuable suggestions.

APPENDIX A: CALCULATION OF THE MIXED TERM

We will only show the calculations for the mixed term $\langle i\mathcal{L}_{12}T_1\rangle_t$ for $D=2$. The calculations in $D=3$ are very similar although slightly longer and the single species terms have already been calculated (see, e.g., [31]). The first steps are straight forward

$$\begin{aligned}\langle i\mathcal{L}_{12}T_1\rangle &= \left\langle \frac{1}{2}\sum_{i,j} i\mathfrak{T}_{12}^{(ij)}T_1\right\rangle \\ &= \frac{1}{2N_1}\sum_{i,j}\left\langle i\mathfrak{T}_{12}^{(ij)}\frac{m_1}{2}\sum_{k=1}^{N_1}\boldsymbol{v}_k^2\right\rangle \\ &= \frac{N_1N_2}{N_1}\left\langle i\mathfrak{T}_{12}^{(12)}\frac{m_1}{2}\boldsymbol{v}_1^2\right\rangle\end{aligned}$$

where we used the molecular chaos assumption to reduce the average over all possible pairs of colliding spheres to a sum of $2N_1N_2$ times the average result of a single colliding pair.

Now we introduce two partitions of unity ($\int d^2R_1d^2R_2\delta(\boldsymbol{R}_1-\boldsymbol{r}_1)\delta(\boldsymbol{R}_2-\boldsymbol{r}_2)$), i.e.

$$\langle i\mathcal{L}_{12}T_1\rangle = N_2\frac{\int \mathrm{d}\Gamma\int \mathrm{d}^2R_1\mathrm{d}^2R_2\delta(\boldsymbol{R}_1-\boldsymbol{r}_1)\delta(\boldsymbol{R}_2-\boldsymbol{r}_2)f_N(\{\boldsymbol{v}_i\},t)i\mathfrak{T}_{12}^{(12)}\frac{m_1}{2}\boldsymbol{v}_1^2}{\int \mathrm{d}\Gamma f_N(\{\boldsymbol{v}_i\},t)}$$

identifying the pair correlation function $g_{12}(R_{12})/V^2=\langle\delta(\boldsymbol{R}_1-\boldsymbol{r}_1)\delta(\boldsymbol{R}_2-\boldsymbol{r}_2)\rangle_t$ in this expression yields

$$\langle i\mathcal{L}_{12}T_1\rangle = \frac{N_2}{V^2}\frac{\int \mathrm{d}^2R_1\mathrm{d}^2R_2\int\prod_j \mathrm{d}^2v_j g_{12}(R_{12})f_N(\{\boldsymbol{v}_i\},t)i\mathfrak{T}_{12}^{(12)}\frac{m_1}{2}\boldsymbol{v}_1^2}{\int\prod_j \mathrm{d}^2v_j f_N(\{\boldsymbol{v}_i\},t)}$$

Substituting $\boldsymbol{R}_{12}=\boldsymbol{R}_1-\boldsymbol{R}_2$ for $\boldsymbol{R}_1$ the other spatial integration is trivial as are all the velocity integrals in the denominator and those for $j>2$ in the numerator:

$$\langle i\mathcal{L}_{12}T_1\rangle = -x_2n\left[\frac{m_1}{2\pi T_1(t)}\right]\left[\frac{m_2}{2\pi T_2(t)}\right]\int \mathrm{d}^2R_{12}\int \mathrm{d}^2v_1\mathrm{d}^2v_2\exp\left[-\frac{m\boldsymbol{v}_1^2}{2T_1}\right]\exp\left[-\frac{m\boldsymbol{v}_1^2}{2T_1}\right]g_{12}(R_{12})i\mathfrak{T}_{12}^{(12)}\frac{m_1}{2}\boldsymbol{v}_1^2$$

Writing $\boldsymbol{R}_{12}$ in polar coordinates such that $\hat{\boldsymbol{R}}_{12}\cdot\boldsymbol{v}_{12}=v_{12}\cos\phi$, the radial integration is simply the application of the δ-function in $\mathfrak{T}_{12}^{(12)}$ and the step function constraints the angular integration.

$$\langle i\mathcal{L}_{12}T_1\rangle = \mathcal{N}\frac{m_1}{2}\int_{\pi/2}^{3\pi/2}\mathrm{d}\phi\int \mathrm{d}^2v_1\mathrm{d}^2v_2v_{12}\cos\phi\exp\left[-\frac{m_1\boldsymbol{v}_1^2}{2T_1(t)}\right]\exp\left[-\frac{m_2\boldsymbol{v}_2^2}{2T_2(t)}\right](b_{12}^{(12)}-1)\boldsymbol{v}_1^2$$

where

$$\mathcal{N}=x_2n(a_1+a_2)\chi_{12}\left[\frac{m_1}{2\pi T_1(t)}\right]\left[\frac{m_2}{2\pi T_2(t)}\right]$$

According to the collision rules, the application of $b_{12}^{(12)}$ yields

$$(b_{12}^{(12)}-1)\boldsymbol{v}_1^2 = -\frac{2\mu}{m_1}(1+\epsilon_{12})(\hat{\boldsymbol{n}}\cdot\boldsymbol{v}_{12})(\hat{\boldsymbol{n}}\cdot\boldsymbol{v}_1)+\frac{\mu^2}{m_1^2}(1+\epsilon_{12})^2(\hat{\boldsymbol{n}}\cdot\boldsymbol{v}_{12})^2$$

where $\mu\equiv\mu_{12}$ is the reduced mass. Introducing the new average

$$\langle A\rangle_2 := \int_{\pi/2}^{3\pi/2}\mathrm{d}\phi\int \mathrm{d}^2v_1\mathrm{d}^2v_2v_{12}\cos\phi A\exp\left[-\frac{m_1\boldsymbol{v}_1^2}{2T_1(t)}\right]\exp\left[-\frac{m_2\boldsymbol{v}_2^2}{2T_2(t)}\right]$$

what we have to calculate is

$$\langle i\mathcal{L}_{12}T_1\rangle = -\mu\mathcal{N}(1+\epsilon_{12})\left\langle(\hat{\boldsymbol{n}}\cdot\boldsymbol{v}_{12})(\hat{\boldsymbol{n}}\cdot\boldsymbol{v}_1)\right\rangle_2 + \frac{\mu^2}{2m_1}\mathcal{N}(1+\epsilon_{12})^2\left\langle(\hat{\boldsymbol{n}}\cdot\boldsymbol{v}_{12})^2\right\rangle_2 \tag{A1}$$

Let's consider the first term in eq. (A1). Substituting $\boldsymbol{v}\equiv\boldsymbol{v}_{12}$ for $\boldsymbol{v}_2$ and writing $\boldsymbol{v}_1$ in polar coordinates such that $\boldsymbol{v}_1\cdot\boldsymbol{v} = v_1 v\cos\gamma$ one gets

$$\begin{aligned}\left\langle(\boldsymbol{v}_{12}\cdot\hat{\boldsymbol{n}})(\boldsymbol{v}_1\cdot\hat{\boldsymbol{n}})\right\rangle_2 = \int \mathrm{d}^2v\int_{\pi/2}^{3\pi/2}d\phi\int_0^\infty dv_1\int_0^{2\pi}d\gamma v^2v_1^2\cos^2\phi\cos(\gamma-\phi)\\ \times\exp\left[-\frac{1}{2}\frac{m_2T_1(t)+m_1T_2(t)}{T_1(t)T_2(t)}v_1^2\right]\exp\left[-\frac{m_2\boldsymbol{v}^2}{2T_2(t)}\right]\exp\left[\frac{m_2v_1v}{T_2(t)}\cos\gamma\right]\end{aligned}$$

Invoking the addition theorem for $\cos(\gamma-\phi)$ the integration over ϕ becomes trivial and the integration over γ defines the associated Bessel function $I_1(x)$.

$$\left\langle(\boldsymbol{v}_{12}\cdot\hat{\boldsymbol{n}})(\boldsymbol{v}_1\cdot\hat{\boldsymbol{n}})\right\rangle_2 = -\frac{8\pi}{3}\int\mathrm{d}^2v\int_0^\infty\mathrm{d}v_1v^2v_1^2I_1(m_2vv_1/T_2(t))\exp\left[-\frac{1}{2}\frac{m_2T_1(t)+m_1T_2(t)}{T_1(t)T_2(t)}v_1^2\right]\exp\left[-\frac{m_2\boldsymbol{v}^2}{2T_2(t)}\right]$$

Integrals of the form $\int\mathrm{d}x x^{n+1}I_n(\alpha x)\exp(-\beta x^2)$ have closed solutions such that we get

$$\left\langle(\boldsymbol{v}_{12}\cdot\hat{\boldsymbol{n}})(\boldsymbol{v}_1\cdot\hat{\boldsymbol{n}})\right\rangle_2 = -\frac{8\pi}{3}\frac{m_2}{T_2(t)}\left[\frac{T_1(t)T_2(t)}{m_2T_1(t)+m_1T_2(t)}\right]^2\int\mathrm{d}^2vv^3\exp\left[-\frac{m_1m_2}{2}\frac{\boldsymbol{v}^2}{m_2T_1(t)+m_1T_2(t)}\right]$$

We are left with a pair of Gaussian integrals. Calculating the second term in eq. (A1) involves essentially the same steps as shown above.

APPENDIX B: SOLVING THE INTEGRAL EQUATIONS

To be able to apply Banach's fix point iteration, we rearrange eqs. (10) and (12) and define operators

$$A_1[T](a) := \frac{-C\int_{R_1}^{R_2}\frac{r^3}{r^3+a^3}(a+r)^2\sqrt{\frac{T(a)}{a^3}+\frac{T(r)}{r^3}}(1+\epsilon)^2\frac{a^3}{a^3+r^3}T(r)\mathrm{d}r - H(a)}{C\int_{R_1}^{R_2}\frac{r^3}{r^3+a^3}(a+r)^2\sqrt{\frac{T(a)}{a^3}+\frac{T(r)}{r^3}}\left[(\epsilon^2-1)-(1+\epsilon)^2\frac{a^3}{a^3+r^3}\right]\mathrm{d}r}$$

and

$$A_2[\omega_0^{-2}](a) := \frac{-C\int_{R_1}^{R_2}\frac{r^3}{r^3+a^3}(a+r)^2\sqrt{\frac{\omega_0^{-2}(a)}{a^3}+\frac{\omega_0^{-2}(r)}{r^3}}(1+\epsilon)^2\frac{a^3}{a^3+r^3}\omega^{-2}(r)\mathrm{d}r - 2\omega_0^{-2}(a)}{C\int_{R_1}^{R_2}\frac{r^3}{r^3+a^3}(a+r)^2\sqrt{\frac{\omega_0^{-2}(a)}{a^3}+\frac{\omega_0^{-2}(r)}{r^3}}\left[(\epsilon^2-1)-(1+\epsilon)^2\frac{a^3}{a^3+r^3}\right]\mathrm{d}r}$$

with $C = n\sqrt{6}/(R_2-R_1)$. Now the solutions of the integral equations are the fix points of A_1 and A_2, which we try to determine by iteration. This method worked well in the case of eq. (10), for ω_0, however, convergence was not fully satisfactory.

That is why we combined it with Newtons method. We define the function G whose root is to be determined by

$$G[f](a) = 2f(a) + C\int_{R_1}^{R_2}\frac{r^3}{r^3+a^3}(a+r)^2\sqrt{\frac{f(a)}{a^3}+\frac{f(r)}{r^3}}\left[(\epsilon^2-1)f(a)+(1+\epsilon)^2\frac{a^3}{a^3+r^3}(f(r)-f(a))\right]\mathrm{d}r$$

and calculate its functional derivative. After discretization of the integrals we obtain a function $G : \mathbb{R}^M \to \mathbb{R}^M$ on which we can apply Newton's method. Newton's method requiring a sufficiently good starting approximation, we chose as such the result of Banach's fixpoint iteration after about 300 iterations.

[1] T. Shinbrot and F. J. Muzzio, Phys. Today **53**, 25 (2000).
[2] I. S. Aranson and L. S. Tsimring, Rev. Mod. Phys. **78**, 641 (2006).
[3] I. Goldhirsch, Annu. Rev. Fluid Mech. **35**, 267 (2003).
[4] J. T. Jenkins and F. Mancini, J. Appl. Mech. **54**, 27 (1987).
[5] J. T. Jenkins and F. Mancini, Phys. Fluids A **1**, 2050 (1989).
[6] V. Garzó and J. Dufty, Phys. Rev. E **60**, 5706 (1999).
[7] H. L. Lu, W. T. Liu, R. S. Bie, L. D. Yang, and D. Gidaspow, Physica A **284**, 265 (2000).
[8] A. Barrat and E. Trizac, Granular Matter **4**, 57 (2002).
[9] S. R. Dahl, C. M. Hrenya, V. Garzó, and J. W. Dufty, Phys. Rev. E **66**, 041301 (2002).
[10] R. Pagnani, U. M. B. Marconi, and A. Puglisi, Phys. Rev. E **66**, 051304 (2002).
[11] M. Alam and S. Luding, J. Fluid. Mech. **476**, 69 (2003).
[12] J. E. Galvin, S. R. Dahl, and C. M. Hrenya, J. Fluid. Mech. **528**, 207 (2005).
[13] M. Alam and S. Luding, Phys. Fluids **17**, 063303 (2005).
[14] V. Garzó and J. M. Montanero, J. Stat. Phys. **129**, 27 (2007).
[15] W. Losert, D. G. W. Cooper, J. Delour, A. Kudrolli, and J. P. Gollub, Chaos **9**, 682 (1999).
[16] P. Zamankhan, Phys. Rev. E **52**, 4877 (1995).
[17] S. R. Dahl, R. Clelland, and C. M. Hrenya, Phys. Fluids. **14**, 1972 (2002).
[18] H. Iddir and H. Arastoopour, AIChE J. **51**, 1620 (2005).
[19] R. Lambiotte and L. Brenig, Phys. Rev. E **72**, 042301 (2005).
[20] V. Garzó, J. W. Dufty, and C. M. Hrenya, Phys. Rev. E **76**, 031303 (2007); a) V. Garzó, C. M. Hrenya, and J. W. Dufty, Phys. Rev. E **76**, 031304 (2007).
[21] C. Zhi-Yuan and Z. Duan-Ming, Chinese Phys. Lett. **25**, 1583 (2008).
[22] D. R. M. Williams and F. C. MacKintosh, Phys. Rev. E **54**, R9 (1996).
[23] A. Prevost, D. A. Egolf, and J. S. Urbach, Phys. Rev. Lett. **89**, 084301 (2002).
[24] I. S. Aranson and J. S. Olafsen, Phys. Rev. E **66**, 061302 (2002).
[25] K. Kohlstedt, A. Snezhko, M. V. Sapozhnikov, I. S. Aranson, J. S. Olafsen, and E. Ben-Naim, Phys. Rev. Lett. **95**, 068001 (2005).
[26] C. C. Maaß, N. Isert, G. Maret, and C. M. Aegerter, Phys. Rev. Lett. **100**, 248001 (2008).
[27] R. P. Ohja, P.-A. Lemieux, P. K. Dixon, A. J. Liu, and D. J. Durian, Nature **427**, 521 (2004).
[28] A. R. Abate and D. J. Durian, Phys. Rev. E **72**, 031305 (2005).
[29] M. Schröter, D. I. Goldman, and H. L. Swinney, Phys. Rev. E **71**, 030301 (2005).
[30] M. Huthmann and A. Zippelius, Phys. Rev. E **56**, R6275 (1997).
[31] T. Aspelmeier, M. Huthmann, and A. Zippelius, in *Granular Gases*, edited by T. Pöschel and S. Luding (Springer Berlin et al., 2001), pp. 31–58.
[32] T. P. C. van Noije and M. H. Ernst, Granular Matter **1**, 57 (1998).
[33] A. Goldshtein and M. Shapiro, J. Fluid Mech. **282**, 75 (1995).
[34] N. V. Brilliantov and T. Pöschel, Phys. Rev. E **61**, 2809 (2000).
[35] M. H. Ernst and R. Brito, in *Granular Gas Dynamics*, edited by T. Pöschel and N. Brilliantov (Springer, 2003), vol. 624 of *Lecture Notes in Physics*, pp. 3–36.
[36] T. Pöschel, N. V. Brilliantov, and A. Formella, Phys. Rev. E **74**, 041302 (2006).
[37] M. A. Hopkins and M. Y. Louge, Phys. Fluids A **3**, 47 (1991).
[38] S. McNamara, Phys. Fluids A **5**, 3056 (1993).
[39] I. Goldhirsch and G. Zanetti, Phys. Rev. Lett. **70**, 1619 (1993).
[40] C. Cattuto and U. M. B. Marconi, Phys. Rev. Lett. **92**, 174502 (2004).
[41] B. D. Lubachevsky, J. Comp. Phys. **94**, 255 (1991).
[42] A. Fiege, T. Aspelmeier, and A. Zippelius, Phys. Rev. Lett. **102**, 098001 (2009).
[43] V. Garzó, Phys. Rev. E **72**, 021106 (2005).
[44] C. Bizon, M. D. Shattuck, J. B. Swift, and H. L. Swinney, Phys. Rev. E **60**, 4340 (1999).
[45] P. K. Haff, J. Fluid. Mech. **134**, 401 (1983).
[46] G. A. Bird, *Molecular Gas Dynamics* (Oxford University Press, London, 1976).
[47] J. J. Brey, M. J. Ruiz-Montero, and D. Cubero, Phys. Rev. E **54**, 3664 (1996).
[48] J. J. Brey, J. W. Dufty, and A. Santos, J. Stat. Phys. **87**, 1051 (1997).
[49] J. M. Montanero and A. Santos, Granular Matter **2**, 53 (2000).
[50] J. J. Brey, M. J. Ruiz-Montero, P. Maynar, and M. I. García de Soria, J. Phys.: Cond. Matt. **17**, S2489 (2005).
[51] P. Español and P. Warren, Europhys. Lett. **30**, 191 (1995).
[52] T. Aspelmeier, W. T. Kranz, and A. Zippelius, in preparation.
[53] A similar scheme is employed in dissipative particle dynamics (see e.g. [51]). For the far reaching consequences the choice of driving mechanism can have, see [42, 52].